SPANDIDOS PUBLICATIONS

INTERNATIONAL JOURNAL OF ONCOLOGY 56: 301-314, 2020

A FXYD5/TGF-β/SMAD positive feedback loop drives epithelial-to-mesenchymal transition and promotes tumor growth and metastasis in ovarian cancer

YANG BAI[1-3*], LIANG-DONG LI[4,5*], JUN LI[1-3], RUI-FANG CHEN[1-3], HAI-LIN YU[1-3], HE-FEN SUN[5,6], JIE-YU WANG[1-3] and XIN LU[1-3]

[1]Department of Gynecology, Obstetrics and Gynecology Hospital of Fudan University, Shanghai 200011; [2]Department of Obstetrics and Gynecology of Shanghai Medical College, Fudan University, Shanghai 200032; [3]Shanghai Key Laboratory of Female Reproductive Endocrine Related Diseases of Fudan University, Shanghai 200011; [4]Department of Neurosurgery, Fudan University Shanghai Cancer Center, Shanghai 200032; [5]Department of Oncology, Shanghai Medical College, Fudan University, Shanghai 200030; [6]Department of Breast Surgery, Key Laboratory of Breast Cancer in Shanghai, Fudan University Shanghai Cancer Center, Shanghai 200030, P.R. China

Received June 3, 2019; Accepted October 2, 2019

DOI: 10.3892/ijo.2019.4911

Abstract. Epithelial ovarian cancer is aggressive and lacks effective prognostic indicators or therapeutic targets. In the present study, using immunohistochemistry and bioinformatics analysis on ovarian cancer tissue data from The Obstetrics and Gynecology Hospital of Fudan University and The Cancer Genome Atlas database, it was identified that FXYD domain-containing ion transport regulator 5 (FXYD5) expression was upregulated in the SKOV3-IP cell line compared with its parental cell line, SKOV3, and in ovarian cancer tissues compared with in normal tissues. In addition, FXYD5 upregulation was predictive of poor patient survival. Furthermore, through various *in vitro* (Transwell assay, clonogenic assay and western blot analysis) and *in vivo* (nude mouse model) experiments, it was demonstrated that FXYD5 promoted the metastasis of ovarian cancer cells. Mechanistically, RNA sequencing, western blot analysis, a luciferase reporter assay and chromatin immunoprecipitation were performed to reveal that FXYD5 dispersed the SMAD7-SMAD specific E3 ubiquitin protein ligase 2-TGF-β receptor 1 (TβR1) complex, deubiquitinated and stabilized TβR1, and subsequently enhanced transforming growth factor-β (TGF-β) signaling and sustained TGF-β-driven epithelial-mesenchymal transition (EMT). The TGF-β-activated SMAD3/SMAD4 complex was in turn directly recruited to the FXYD5 promoter region, interacted with specific SMAD-binding elements, and then promoted FXYD5 transcription. In brief, FXYD5 positively regulated TGF-β/SMADs signaling activities, which in turn induced FXYD5 expression, creating a positive feedback loop to drive EMT in the process of ovarian cancer progression. Collectively, the findings of the present study suggested a mechanism through which FXYD5 serves a critical role in the constitutive activation of the TGF-β/SMADs signaling pathways in ovarian cancer, and provided a promising therapeutic target for human ovarian cancer.

Correspondence to: Dr Xin Lu, Department of Gynecology, Obstetrics and Gynecology Hospital of Fudan University, 419 Fangxie Road, Shanghai 200011, P.R. China
E-mail: xinluktz@163.com

[*]Contributed equally

Abbreviations: EOC, epithelial ovarian cancer; TGF-β, transforming growth factor-β; TβR1, TGF-β receptor 1; EMT, epithelial-mesenchymal transition; FXYD5, FXYD domain-containing ion transport regulator 5; SMAD7, SMAD family member 7; SMURF2, SMAD specific E3 ubiquitin protein ligase 2; TCGA, The Cancer Genome Atlas; IHC, immunohistochemistry; SBEs, SMAD-binding elements

Key words: FXYD domain-containing ion transport regulator 5, transforming growth factor-β/SMADs signaling, epithelial-mesenchymal transition, epithelial ovarian cancer, metastasis

Introduction

Metastasis remains a major challenge in the clinical management of ovarian cancer, and an improved mechanistic understanding of ovarian cancer metastasis and more effective therapeutic approaches for metastatic disease are urgently required (1).

Before the epithelial ovarian cancer (EOC) cells detach and begin metastasizing, they commonly undergo epithelial-mesenchymal transition (EMT), a process through which epithelial cells lose their cell polarity and gain invasive properties to become mesenchymal-like cells (2). Typically, in cancer cells, EMT can be triggered by transforming growth factor-β (TGF-β), which facilitates tumorigenesis and metastasis in the late stages of cancer progression, including in EOC (2-6).

TGF-β binds to serine/threonine kinase receptors (TβR1/TβR2) at the cell membrane, and activates a signaling cascade by phosphorylating specific receptor-regulated SMADs, namely, SMAD2 and SMAD3 (7). Phosphorylated SMAD2/3 forms a complex with SMAD4 and shuttles to the nucleus to activate the transcription of downstream effectors (7,8). Furthermore, SMAD7 acts as a bridge protein by recruiting SMAD specific E3 ubiquitin protein ligase 2 (SMURF2), an E3 ubiquitin ligase, to the TGF-β receptor complex, which subsequently results in the proteasomal-mediated degradation of TβR1, thereby attenuating TGF-β signaling (9,10).

FXYD domain-containing ion transport regulator 5 (FXYD5) has been identified as a cancer-associated protein whose expression inhibits E-cadherin and promotes metastasis (11-13). As a single span type I membrane protein and an auxiliary subunit of the Na^+/K^+-ATPase, FXYD5 also modulates cellular junctions and adhesion through the regulation of the β-Na^+-K^+-ATPase subunit (12-16). Additionally, Nam *et al* (17) have reported that C-C motif chemokine ligand mediates the pro-metastatic effect of FXYD5 in human breast cancer cells.

However, to date, few studies have systematically examined the functional significance of FXYD5 in a clinical setting or in the molecular behavior of ovarian cancer (12,18,19). In addition, to the best of our knowledge, there are no studies which have linked FXYD5 to the TGF-β signaling pathway. The present study demonstrated that FXYD5 forms a positive feedback loop with TGF-β to drive EMT and promote metastasis in ovarian cancer *in vitro* and *in vivo*.

Materials and methods

Bioinformatics analysis. All The Cancer Genome Atlas (TCGA) (https://portal.gdc.cancer.gov/) data and figures were accessed, analyzed and generated using the Ovarian Serous Cystadenocarcinoma (TCGA, Provisional) database from cBio Cancer Genomics Portal (http://cbioportal.org) (20). All data included in this manuscript are in agreement with the TCGA publication guidelines. The present study utilized datasets (including Bonome Ovarian, Bittner Ovarian 2005, Badea Pancreas 2008, DErrico Gastric 2009, Gumz Renal 2007, He Thyroid 2005, Korkola Seminoma 2006 and TCGA Colorectal 2011) from the Oncomine database (http://www.oncomine.org), an online microarray database and web-based data-mining platform that comprises transcriptome data, to compare the FXYD5 mRNA expression differences between normal and tumor tissues of multiple types of human cancer. The Kaplan-Meier Plotter (http://kmplot.com/analysis/) was utilized to calculate the probability of disease progression, and the analysis included 1,648 patients with ovarian cancer with a mean follow-up period of 40 months (21). Using TFSEARCH (http://www.cbrc.jp/research/db/TFSEARCH), four putative transcriptional factor binding sites, including SMAD-binding element (SBE)1, SBE2, SBE3 and SBE4, which were located in the -1439/+4 FXYD5 promoter region, were identified.

Study population. The present study included 58 patients who were diagnosed with pathologically high-grade and stage III serous ovarian cancer and 22 patients who were diagnosed with a benign ovarian tumor or other benign uterine lesions and underwent prophylactic adnexectomy between March 2015 and October 2016 at the Obstetrics and Gynecology Hospital of Fudan University (Shanghai, China). All patients were female, and aged between 27 and 67 years (average age, 41.8 years). Two experienced and independent pathologists from the Pathology Department at the Obstetrics and Gynecology Hospital of Fudan University (Fudan, China) verified the diagnoses. Approval was obtained from the Human Research Ethics Committee of the Obstetrics and Gynecology Hospital of Fudan University for the use of all samples by using a protocol that conforms to the provisions of the Declaration of Helsinki (as revised in Seoul, 2008; reference no. [2015] 27).

In vivo experiments. A total of 50 female BALB/c nude mice (age, 4-6 weeks; weight, 13-15 g; n=6-10 mice/group) were used in the present study according to a standard protocol that was approved by the Institutional Animal Care and Use Committee of Fudan University. The mice were purchased from SLAC Laboratory Animal Co., Ltd. (SCXK-2007-004) and maintained at 22±2˚C under a 12-h light/dark cycle in a pathogen-free environment. All mice were freely accessed autoclaved standard food and water. For nude mouse xenograft assays, SKOV3 cells ($3x10^6$ per mouse) transfected with the FXYD5 overexpression lentivirus or control plasmid vector were suspended in 100 μl PBS and injected subcutaneously into mice on the right side of their backs. The body weight and tumor volume (V) (calculated using the formula V=length x width x thickness in mm^3 to estimate the actual volume of the tumors) were monitored 3 times per week. For intraperitoneal metastasis assays, SKOV3-IP cells ($7x10^6$/0.2 ml PBS per) transfected with the FXYD5 silencing lentivirus or control plasmid vector were injected intraperitoneally into each mouse. After 3-4 weeks, tumors were surgically excised.

Cell lines. Ovarian cancer cell lines, including SKOV3, OVCAR3, OVCA433, A2780, HEY and CAOV3, were obtained from the American Type Culture Collection. The metastatic human serous ovarian cancer cell line, SKOV3-IP, was obtained from the M.D. Anderson Cancer Center (Houston, TX, USA). The 293T cell line, which was authenticated by applying the short tandem repeat profiling method each year, was obtained from the Shanghai Cell Bank, Type Culture Collection Committee of Chinese Academy of Science. All preserved cell lines in the laboratory underwent routine cell quality examinations by HD Biosciences Co., Ltd. to achieve a high-quality cellular standard. The ovarian cancer cell lines were maintained in RPMI-1640 supplemented with 10% FBS (Gibco; Thermo Fisher Scientific, Inc.), 100 IU/ml penicillin, and 100 mg/ml streptomycin. 293T cells were grown in DMEM (Corning Inc.) supplemented with 10% FBS (Gibco; Thermo Fisher Scientific, Inc.), 100 IU/ml penicillin, and 100 mg/ml streptomycin. All cells were cultured in an incubator at 37˚C with 5% CO_2.

Cellular treatment. TGF-β (0-10 ng/ml; cat. no. AF-100-21C; PeproTech, Inc.) was used to activate the TGF-β pathway

in control SKOV3 cells and in SKOV3 cells overexpressing FXYD5. Cyclohexane (CHX; cat. no. 5087390001; Sigma-Aldrich; Merck KGaA) was used to inhibit protein synthesis and MG132 (10 μM; cat. no. M8699-1MG; Sigma-Aldrich; Merck KGaA) was used to inhibit protein degradation through the proteasome pathway in control and FXYD5-overexpressing SKOV3 cells.

Immunohistochemistry (IHC) and IHC variable evaluation. Ovarian cancer and normal ovarian tissues were fixed in 10% formalin at room temperature for 24 h, dehydrated in an ascending series of alcohol (70, 85, 95 and 100%) and xylene, embedded in paraffin and sliced into 3-μm sections. Subsequently, sections of paraffin-embedded tissues (3-μm thick) were deparaffinized in dimethylbenzene and rehydrated in a descending series of alcohol (100, 95, 85 and 70%) and distilled water. Endogenous peroxidase activity was quenched using 10-30% hydrogen peroxide in methanol at room temperature for 15 min. Subsequently, antigen retrieval was conducted using citric acid buffer (pH 6.0) at 99˚C for 30 min followed by cooling for 20 min, and blocking in 5% BSA (cat. no. SW3015; Beijing Solarbio Science & Technology Co., Ltd.) for 1 h at room temperature. The tissue was incubated in primary anti-FXYD5 antibody (1:500; cat. no. 12166-1-AP; ProteinTech Group, Inc.), anti-β-catenin (1:400; cat. no. 8480; Cell Signaling Technology, Inc.) and vimentin (1:500; cat. no. 5741; Cell Signaling Technology, Inc.) overnight at 4˚C. Incubation with the biotinylated secondary antibody (rabbit IgG; 1:1,000-3,000; cat. no. 7074; Cell Signaling Technology, Inc.) was followed by the addition of horseradish peroxidase. Counterstaining was performed using hematoxylin at room temperature for 1 min. Images were acquired using a Leica TCS SP2 confocal laser-scanning microscope (Leica Microsystems, Inc.). For quantification, overall immunostaining scores were calculated using the H-Score system (22). The same procedure was applied for tissues from the mouse in situ and metastatic tumors.

Plasmids and short hairpin RNA (shRNA). Human FXYD5 cDNA was subcloned from the SKOV3 ovarian cancer cell line into the pCDH-CMV-MCS-EF1-Puro lentiviral vector. The cloned primer sequence is shown in Table SI. Human FXYD5 shRNA and the negative control, which were expressed in the GV248 backbone, were obtained from GeneChem, Inc. Among five identified shRNAs, the two most effective were used for further experiments, and the target sequences are presented in Table SI.

Reverse transcription-quantitative PCR (RT-qPCR). Total RNA was extracted from cultured cells using the TRIzol® reagent (Invitrogen; Thermo Fisher Scientific, Inc.) and RT-qPCR was performed with GAPDH as an internal control. Total RNA was then reverse transcribed into cDNA using the Prime-Script RT Reagent kit (Takara Bio, Inc.). RT was performed using 2.0 μl 5X gDNA Eraser Buffer, 1.0 μl gDNA Eraser, 1 μg Total RNA and RNase Free dH_2O, to a total volume of 10 μl. The volume was maintained at 42˚C for 2 min and was then rapidly cooled to 4˚C. Subsequently, the aforementioned 10.0 μl reaction solution was mixed with 1.0 μl PrimeScript RT Enzyme Mix 1, 1.0 μl RT Primer Mix, 4.0 μl 5X PrimeScript Buffer 2 and 4.0 μl RNase Free dH_2O. The reaction conditions were as follows: 37˚C for 15 min, 85˚C for 5 sec, followed by cooling to 4˚C and storage at -20˚C. qPCR was then performed using SYBR Premix Ex Taq (Takara Bio, Inc.) according to the manufacturer's instructions. The thermocycling conditions were as follows: Denaturation for 10 sec at 95˚C, followed by 40 cycles of amplification at 95˚C for 15 sec and 60 sec at 34˚C, and a final extension step at 72˚C for 1 min. qPCR was performed on the ABI Prism 7500 instrument (Applied Biosystems; Thermo Fisher Scientific, Inc.). A fluorescence-based qPCR method was performed using 2 μl cDNA, 10 μl SYBR Green, 0.6 μl PCR forward primer (10 μM), 0.6 μl PCR reverse primer (10 μM) and 6.8 μl dH_2O in a 20-μl PCR reaction volume. GAPDH was used as a reference gene, and the data were normalized using the standard comparative C_q method (23). The specific primers that were used in the present study are listed in Table SI.

Lentivirus packaging and infection. Briefly, the 293T cells (cells growing to 80% confluence) were co-transfected with lentiviral vectors (PCDH or GV248) and the packaging vectors (psPAX2 and pMD2G), as described previously (24).

RNA interference. The SKOV3 and SKOV3-IP cells (cells growing to 30-50% confluence) were transfected with 50 nM small interfering RNA (siRNA) that targeted corresponding genes or 50 nM scrambled negative control (Shanghai GenePharma Co., Ltd.) using the HiPerFect Transfection reagent (Qiagen GmbH) according to the manufacturer's instructions. Following 48 h of transfection, the cells were collected for use in further experiments. The targeting sequences of the siRNAs and negative control are listed in Table SI.

RNA sequencing analysis. Total RNA was extracted from FXYD5-overexpressing and control SKOV3 cells using TRIzol® reagent (Invitrogen; Thermo Fisher Scientific, Inc.). Quantified total RNA was further purified using the RNeasy Micro kit (cat. no. 74004; Qiagen GmbH) and RNase-Free DNase Set (cat. no. 79254; Qiagen GmbH) and then used for Solexa/Illumina sequencing (Shanghai Biotechnology Corp.). Hg38 RefSeq (RNA sequences, GRCh38) was downloaded from the UCSC Genome Browser (http://genome.ucsc.edu). Kyoto Encyclopedia of Genes and Genomes and Gene Ontology enrichment analyses were performed on the differentially expressed genes, which were defined as genes with changes in expression of >2 or <0.5 and a false discovery rate Q value (adjusted P-value) <0.05. Data analysis was performed utilizing FunRich (version 3), an open access standalone functional enrichment and interaction network analysis tool (25).

Western blot analysis. Briefly, whole cell extracts were prepared in chilled RIPA lysis buffer (Beyotime Institute of Biotechnology) containing protease inhibitor cocktail (Roche Diagnostics), as well as phosphatase inhibitors (Sangon Biotech Co., Ltd.). The protein concentration of the supernatants was then measured using a bicinchoninic acid (BCA) assay reagent kit (Thermo Fisher Scientific, Inc.). For western blot analysis, 40 μg total cell lysate, either from ovarian cancer

cell culture or from ovarian tumor tissues, was subjected to SDS-PAGE (8-12% gels) and transferred to 0.45 or 0.22-μm PVDF membranes (EMD Millipore). The membranes were blocked with 5% milk or 5% BSA at room temperature for 60 min or at 4˚C overnight, followed by incubation with the indicated primary antibodies overnight at 4˚C. The membranes were then incubated with the appropriate horseradish peroxidase-conjugated secondary antibodies (Cell Signaling Technology, Inc.) at room temperature for 2 h, and finally identified using an ECL Western Blotting system (Pierce; Thermo Fisher Scientific, Inc.). Densitometric analyses of the immunoblots were conducted using ImageJ software (version 1.50i; National Institutes of Health). All antibodies used in the present study are presented in Table SII.

Transwell assays. Briefly, $4x10^4$ ovarian cancer cells were plated in the top chamber with the non-coated membrane (8-μm pore size; Corning Life Sciences) for migration assays and with Matrigel-coated membrane (8-μm pore size; BD Biosciences) for invasion assays in 200 μl serum-free DMEM. DMEM containing 20% FBS was used as a chemo-attractant in the lower chamber. Following incubation for 10-24 h at 37˚C, the cells which did not traverse through the pores in the top layer were removed with a sterile cotton swab, whereas the remaining cells on the lower surface of the membrane were fixed with methanol and stained with 0.1% crystal violet (Sigma-Aldrich; Merck KGaA) at room temperature for 30 min. The number of migratory and invasive cells was counted in five randomly selected fields of each chamber under a light microscope (Nikon Corporation; magnification, x200), and an average number of cells was then calculated.

Clonogenic assay. After 7 days of growth, cell survival was evaluated by the addition of 500 cells/well to 6-well plates, fixing the cells with methanol and staining of the cells with 1% crystal violet at room temperature for 30 min. Colonies were recorded using ImageJ software (version 1.50i; National Institutes of Health).

ELISA. The TGF-β levels in the conditioned media were measured using the human TGF-β1 ELISA kit (cat. no. ELH-TGFb1-1; RayBiotech, Inc.) according to the manufacturer's protocol.

Immunofluorescence. SKOV3 stably transfected cell lines grown on glass culture slides were fixed with 4% paraformaldehyde for 10 min at room temperature, followed by permeabilization with 0.5% Triton X-100 for 5 min. Subsequently, the cells were blocked with 5% BSA at room temperature for 1 h, and then incubated with primary antibodies against N-cadherin, E-cadherin and vimentin (1:200 dilution; Cell Signaling Technology, Inc.) overnight at 4˚C. The slides were incubated with Alexa Fluor 488-conjugated secondary antibody (1:500 dilution; Invitrogen; Thermo Fisher Scientific, Inc.) for 40 min at room temperature. The immunofluorescence of the cytoskeleton was performed by incubation with rhodamine-conjugated phalloidin (Sigma-Aldrich; Merck KGaA) at room temperature for 40 min. Following counterstaining with DAPI for 10 min at room temperature; images were captured under a confocal microscope (Leica TCS SP5 II; Leica Microsystems, Inc.). All antibodies used in the present study are presented in Table SII.

Immunoprecipitation. Control and FXYD5-overexpressing SKOV3 cells ($4x10^6$ per group) were treated with MG132 (10 μM; cat. no. M8699-1MG; Sigma-Aldrich; Merck KGaA) at room temperature for 4 h to block proteasome activity. They were then lysed with RIPA lysis buffer (Beyotime Institute of Biotechnology) containing protease inhibitor cocktail (Roche Diagnostics) and phosphatase inhibitors (Sangon Biotech Co., Ltd.), and the lysates were centrifuged at 12,000 x g for 10 min at 4˚C. The protein concentrations were measured using a bicinchoninic acid assay reagent kit (Thermo Fisher Scientific, Inc.), and equal amounts of the lysates were used for immunoprecipitation. Thereafter, the cell lysates were immunoprecipitated overnight at 4˚C with an anti-TβR1 antibody, and the protein A/G beads were mixed with the immunoprecipitates, followed by incubation at 4˚C for 3 h. The precipitates were collected by centrifugation at 10,000 x g at 4˚C for 2 min and washed three times with washing buffer. The immunoprecipitated protein complex was separated by SDS-PAGE (8-12% gels), followed by immunoblotting overnight at 4˚C with anti-ubiquitin antibody to detect polyubiquitinated TβR1 proteins.

The present study utilized co-immunoprecipitation to test the formation of the SMURF2-SMAD7-TβR1 complex. As aforedescribed, cell lysates were incubated overnight at 4˚C with an anti-TβR1 antibody, the complex was conjugated to protein A/G sepharose beads, and the beads were collected and washed with lysis buffer and subjected to SDS-PAGE. Where indicated, the cell lysates were immunoprecipitated overnight at 4˚C with the anti-SMURF2 and anti-SMAD7 antibodies (Santa Cruz Biotechnology, Inc.). All antibodies used in the present study are presented in Table SII.

Luciferase reporter assay. The promoter sequence of FXYD5 was synthesized by GeneCopoeia, Inc. A series of truncated FXYD5-promoter luciferase constructs were generated according to the predicted SMAD2-SMAD3-SMAD4 complex binding sites for FXYD5 promoter in Jaspar (http://jaspar.genereg.net). In the luciferase reporter assays, 293T cells were seeded on 24-well plates at a density of $1x10^5$ cells/well and transfected with PGL3-Promoter 0, 1, 2, 3 or 4 (P0, P1, P2, P3 or P4), together with the *Renilla* pRL-TK plasmid (a normalizing control; Promega Corporation), using FuGENE HD Transfection Reagent (Promega Corporation), according to the manufacturer's protocol. The cells were then treated with or without 10 ng/ml TGF-β for 24 h. Sequences, such as P0, P1, P2, P3 and P4, that contained truncated promoter regions of FXYD5 were amplified and subcloned into the PGL3-Basic Vector (Promega Corporation). After 48 h, cells were harvested, and the luciferase activities were determined using the Dual-Glo® Luciferase Assay system with a Modulus™ single tube multimode reader (Turner BioSystems; Thermo Fisher Scientific, Inc.) at 595 nm. The relative firefly luciferase activities were obtained by normalizing the firefly luciferase activity level to the *Renilla* luciferase activity level. Promoter and primer sequences for the construction of the specific plasmid are listed in Tables SIII and SIV.

Chromatin immunoprecipitation (ChIP). ChIP assays were performed using the EZ-Magna ChIPTM Chromatin Immunoprecipitation kit (EMD Millipore) according to the manufacturer's protocol. Briefly, immunoprecipitation was conducted by mixing the samples with the anti-p-SMAD3 and anti-SMAD4 antibodies (Cell Signaling Technology, Inc.) (incubating overnight at 4˚C). Rabbit IgG was used as a negative control. Purified ChIP DNA segments were used as templates for qPCR, which was conducted using SYBR Premix Ex Taq (Takara Bio, Inc.) and the ABI Prism 7500 instrument (Applied Biosystems; Thermo Fisher Scientific, Inc.). The RT-qPCR conditions were as follows: Pre-heating for 10 sec at 95˚C, followed by 40 cycles at 95˚C for 15 sec and 60 sec at 34˚C, and final extension at 72˚C for 1 min. qPCR was used to amplify the FXYD5 promoter regions, SBE1-4. The specific ChIP primers that were used to measure the enrichment of the putative SMAD3/4 binding sites in the FXYD5 promoter are listed in Table SI. All antibodies used in the present study are presented in Table SII.

Statistical analysis. Unless otherwise specified, data are presented as the mean ± SD of at least three independent experiments. Statistical analyses were performed using PRISM v6.0 (GraphPad Software, Inc.) and SPSS v16.0 software (SPSS, Inc.). Student's t-test was used to compare quantitative data between two groups, and one-way analysis of ANOVA with Dunnett's or Least-Significant Difference post hoc tests were used to compare the means among multiple groups. Spearman's correlation analysis was used to analyze the correlation between FXYD5 and TGFB1, and FXYD5 and TGF-β-induced transcript 1 (TGFB1I1) expression. The Kaplan-Meier method and log-rank test were used to plot the survival curves. $P<0.05$ was considered to indicate a statistically significant difference.

Results

FXYD5 is upregulated in advanced-stage EOC and predicts poor survival in patients with ovarian cancer. First, the present study confirmed that FXYD5 expression was upregulated in the SKOV3-IP cell line, which is an *in vivo* passaged variant of SKOV3 cells established by Yu *et al* that exhibits a more malignant phenotype, with higher cell growth and DNA synthesis rates, when compared with its parental SKOV3 cell line (26) (Fig. 1B). Notably, in a subset of patients (stage III EOC, n=58; normal, n=22) treated at the Obstetrics and Gynecology Hospital of Fudan University, who were diagnosed with a benign ovarian tumor or other benign uterine lesions and underwent prophylactic adnexectomy from March 2015 to October 2016. it was observed that 45 (77.6%) of the tumor samples scored as moderate-strong, whereas 3 (13.6%) normal samples scored as moderate-strong for FXYD5 protein expression (Fig. 1C and D).

Among the 591 patients from the TCGA database, 70 cases (12%) presented with FXYD5 alterations, including gene amplification (n=58), mRNA upregulation (n=19), and gene deletions (n=1; Fig. 1E). One mechanism for the induction of high FXYD5 expression in EOC cases could be copy number aberrations (Fig. S1A). Additionally, genomic alterations of FXYD5 were associated with a poor survival rate (Fig. 1E).

Furthermore, large-scale data analysis using the Kaplan-Meier plotter indicated that FXYD5 mRNA upregulation was associated with poor overall, relapse-free and post-progression survival in patients with EOC [hazard ratio (HR)=1.59, 95% CI, 1.26-2.0, $P=7.2\times10^{-5}$, n=655; HR=1.69, 95% CI, 1.37-2.08, $P=5.2\times10^{-7}$, n=614; and HR=1.58, 95% CI, 1.24-2.01, $P=1.8\times10^{-4}$, n=382, respectively; Fig. 1F]. An intrinsic subtype and clinicopathological feature analysis revealed that the effect of FXYD5 mRNA expression on patient survival may be influenced by the histological subtype, clinical stage and debulking surgery (Fig. S1F; Tables SV-SVII). Notably, for patients treated with chemotherapy (single or combination treatment with platinum and Taxol; Tables SV-SVII) or other types of malignant tumors (Fig. S1G), high FXYD5 expression indicated a poor survival.

Subsequently, to examine whether FXYD5 was upregulated specifically in EOC, an analysis of additional independent datasets in the TCGA and Oncomine platforms was performed, and it was revealed that FXYD5 expression was elevated in various types of human cancer (Fig. S1B-E).

Overall, these data suggested that FXYD5 may serve oncogenic and metastasis-promoting roles in ovarian cancer, making FXYD5 an interesting target for further investigation.

FXYD5 promotes ovarian cancer metastasis and tumor growth in vitro and in vivo. To investigate the role of FXYD5 in tumor migration and metastasis, three EOC cell line models, in which FXYD5 was overexpressed or knocked down, were established for *in vitro* and *in vivo* experiments (Fig. 2A).

Notably, in the SKOV3 and CAOV3 cell lines with relatively low levels of endogenous FXYD5 expression (Fig. 1B), FXYD5 overexpression significantly promoted cell migration and invasion in Transwell assays (Fig. 2A and B). Using a complementary inverse approach, FXYD5 deletion suppressed the migratory and invasive abilities of the SKOV3-IP cells *in vitro* (Fig. 2A and B).

Subsequently, the present study examined the effects of FXYD5 on cancer cell dissemination *in vivo*. Notably, the FXYD5-overexpressing group formed more disseminated nodules (12 vs. 5 intraperitoneal nodules on average for the test and control groups) than the control group (n=14; Fig. 2C). Additionally, IHC analysis of the intraperitoneal nodules revealed that, compared with the control tumors, the FXYD5 tumors exhibited a robust ectopic FXYD5 overexpression, with lower β-catenin expression and higher vimentin expression (Fig. 2C).

Additionally, colony formation assays demonstrated that FXYD5 overexpression could significantly promote colony formation of SKOV3 cells, whereas the loss of FXYD5 expression inhibited the colony formation of SKOV3-IP cells (Fig. 2D).

Furthermore, the present study established a xenograft model of ovarian cancer to examine the effects of FXYD5 on tumor growth in vivo. The sizes of the tumors, which were dissected from each mouse, were markedly larger in the FXYD5 group than in the control group (Fig. 2E). Consistently, the average tumor weight was considerably greater in the FXYD5 group, with a 2.5-fold change compared with the control group (Fig. 2E). By day 21, the estimated tumor volume

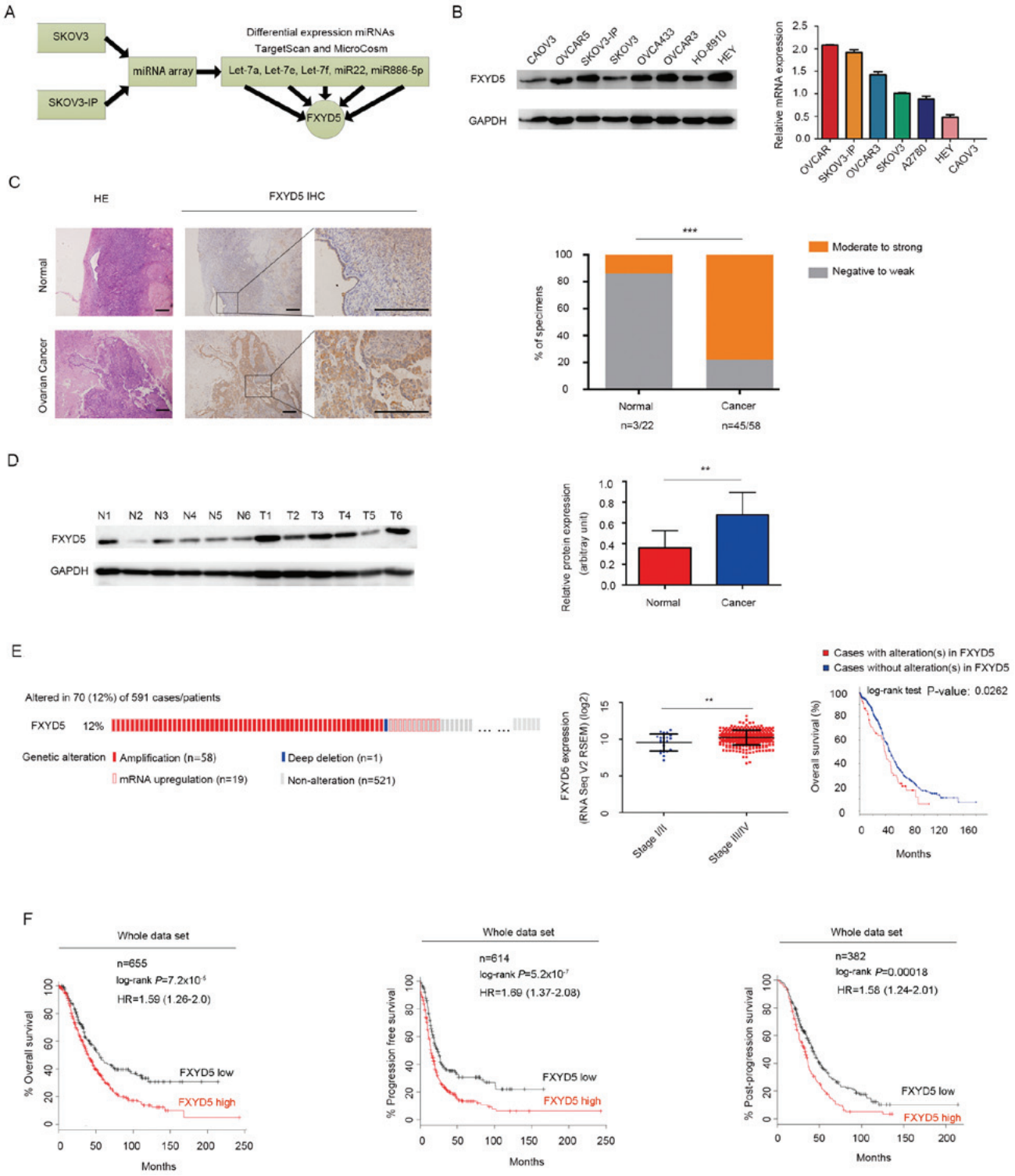

Figure 1. FXYD5 is upregulated in advanced stage EOC and predicts poor survival in patients with ovarian cancer. (A) FXYD5 was the common target gene of the screened miRNAs that were potential suppressors of EOC metastasis. (B) Protein and mRNA expression of FXYD5 in EOC cell lines. (C) Representative images of FXYD5 immunohistochemistry are shown in the large and small images. The percentages of specimens displaying negative-to-weak and moderate-to-strong FXYD5 protein expression are presented on the right. Scale bar, 20 μm. (D) Western blot analysis of FXYD5 protein expression in ovarian cancer and normal tissues. Histogram comparing FYXD5 protein expression between tumor and normal samples. (E) FYXD5 gene alterations in the cohort of patients with ovarian cancer from the TCGA dataset (n=591), including amplification (n=58; 9.81% of total cases), mRNA upregulation (n=19; 3.2% of total cases) and gene deletion (n=1; 0.17% of total cases). FXYD5 mRNA expression was significantly higher in the later than the earlier stages of EOC. Patients harboring FXYD5 alterations exhibited poor overall survival. (F) Expression and survival analysis of FXYD5 mRNA in patients with ovarian cancer using an online Kaplan-Meier plotter. Statistical analysis was performed using Student's t-test (n≥3). The error bars represent the SD. **P<0.01; ***P<0.001; ns, no significant difference. EOC, epithelial ovarian cancer; FXYD5, FXYD domain-containing ion transport regulator 5; HE, hematoxylin and eosin; miRNA, microRNA; N, normal; T, tumor.

in the FXYD5 group was almost 3-fold greater than that in the control group (Fig. 2E). Conversely, FXYD5 silencing inhibited SKOV3-IP cell survival and tumor growth *in vivo*, as shown in Fig. 2F. Collectively, these data demonstrated that

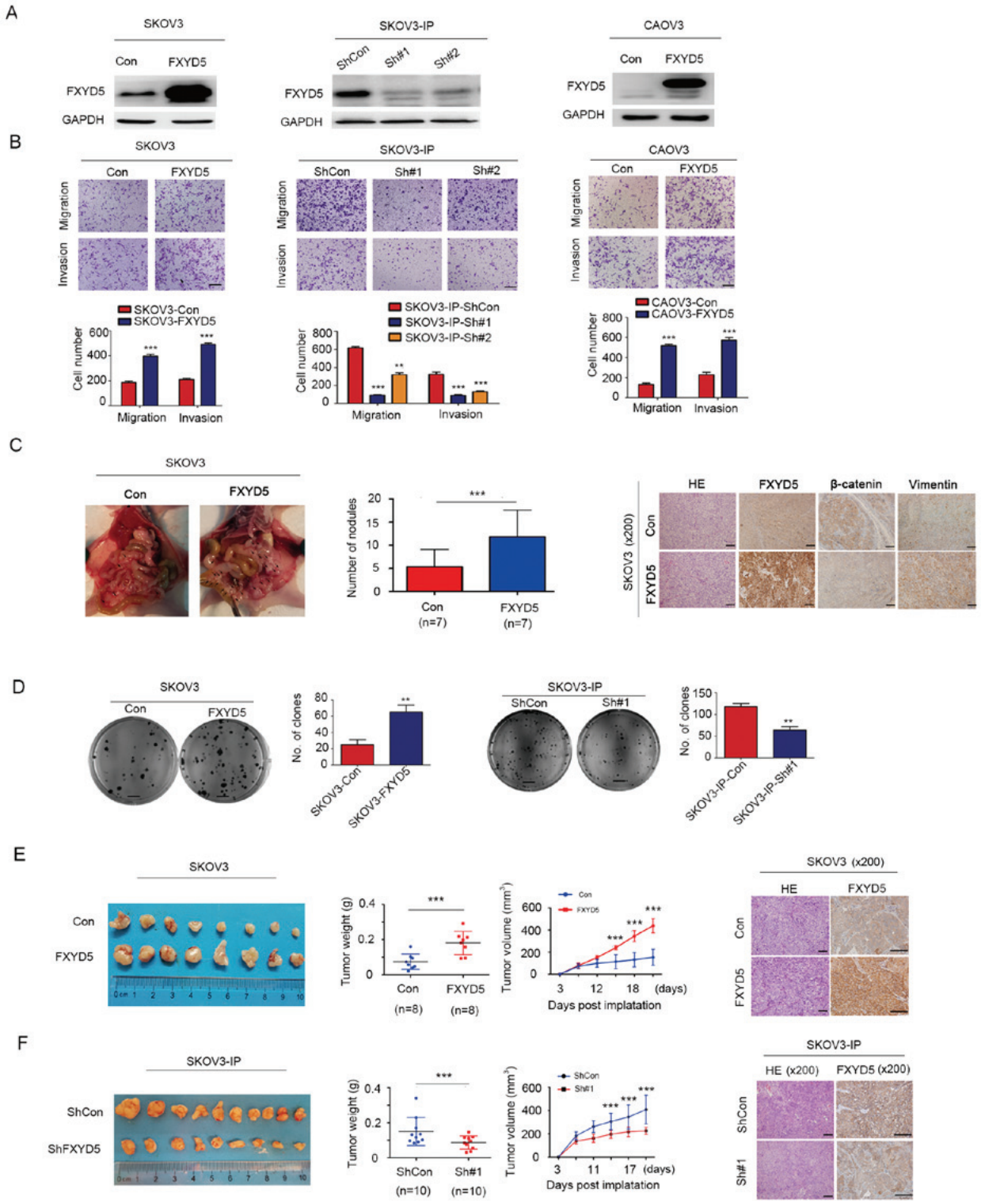

Figure 2. FXYD5 promotes ovarian cancer metastasis and tumor formation *in vitro* and *in vivo*. The migration and invasion abilities of each cell line were evaluated by Transwell assays *in vitro*. (A) FXYD5 protein overexpression or knockdown effects in cell lines, including SKOV3, SKOV3-IP and CAOV3. (B) Upper panel, images of representative fields of invasive cells. Magnification, x10. Scale bar, 10 μm. Lower panel, histograms of the results. **P<0.01; ***P<0.001 vs. SKOV3-IP-ShCon. (C) Whole-enterocoelia images and quantification of metastasis nodules in the peritoneal cavity on day 28 after intraperitoneally injection of SKOV3 cells (n=10 mice per group). Arrows indicate metastasis nodules. HE and IHC staining for FXYD5, β-catenin and vimentin in representative control and FXYD5 tumors. Magnification, x200. Scale bar, 40 μm. (D) Clonogenic assays to assess cellular survival in ectopic FXYD5 expression SKOV3 cells and endogenous FXYD5 silencing SKOV-IP cells. Fold changes in number of colonies for ectopic FXYD5 cells vs. control and control vs. FXYD5 silencing cells (right). Scale bar, 500 μm. **P<0.01. (E and F) Ovarian tumors were removed and collected from the control, ectopic FXYD5 and FXYD5 deletion mice (n=8-10 per group) 28 days post-orthotopic implantation (left). The estimated tumor weight (g) and tumor volume (mm^3) were measured twice per week (middle). HE and IHC staining for FXYD5 in representative mouse tumors (right). Scale bar, 40 μm. (E) ***P<0.001 D12 vs. D15, D15 vs. D18 and D18 vs. D21; (F) ***P<0.001 D11 vs. D14, D14 vs. D17 and D17 vs. D20. Student's t-test was used to compare quantitative data between two groups, and one-way ANOVA with Least-Significant Difference [E, tumor volume, D15 compared with D18 and D18 compared with D21; F, tumor volume, D14 compared with D17 and D17 compared with D20] or Dunnett's (B, SKOV3-IP-ShCon compared with SKOV3-IP-Sh#1 and SKOV3-IP-Sh#2) post hoc tests were used to compare the means among multiple groups (n>3). The error bars represent the SD. ***P<0.001; ns, no significant difference. Con, control; FXYD5, FXYD domain-containing ion transport regulator 5; HE, hematoxylin and eosin; IHC, immunohistochemistry; sh, short hairpin RNA; IP, immunoprecipitation.

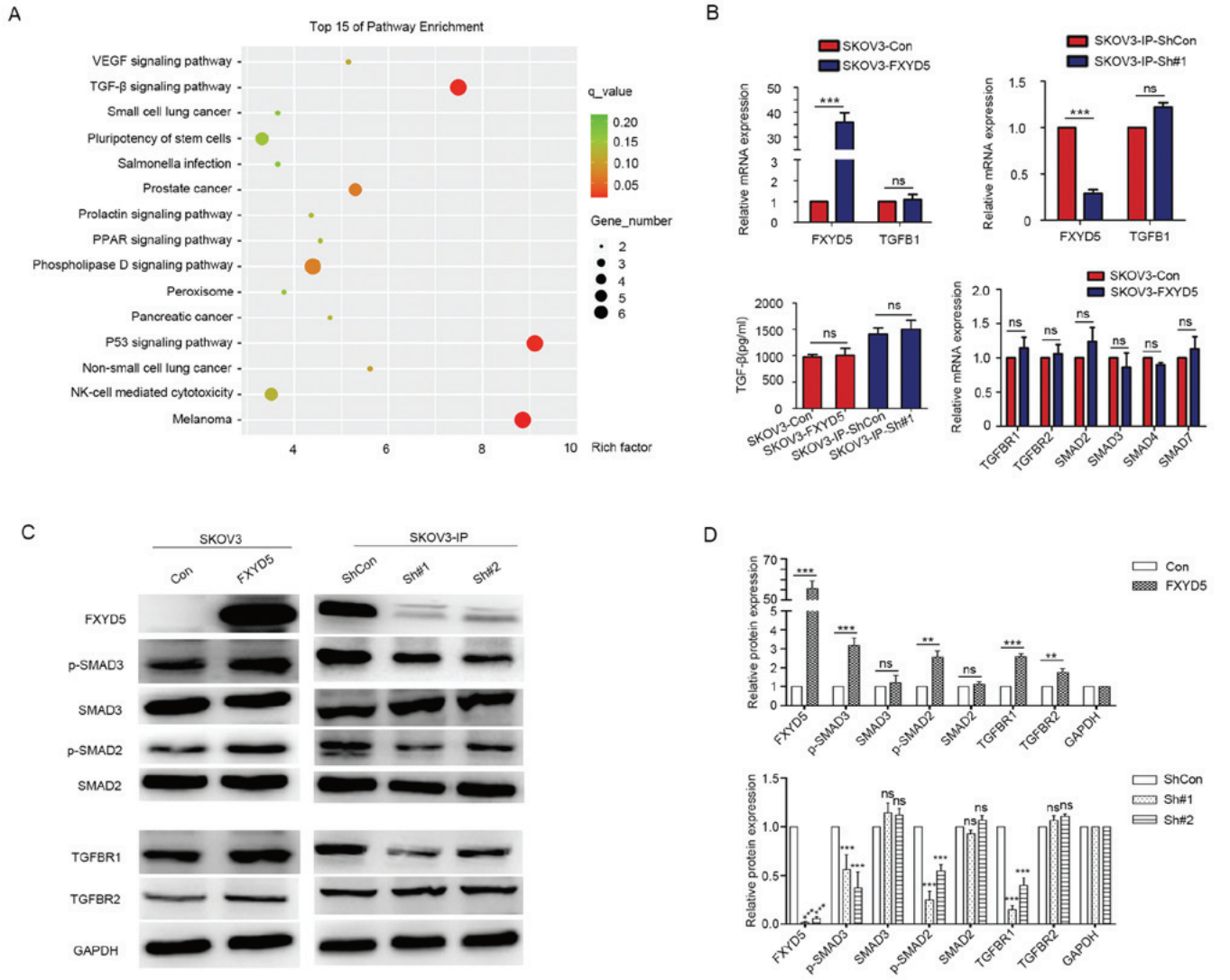

Figure 3. FXYD5 activates TGF-β/SMADs signaling *in vitro*. (A) Global canonical pathway analysis. Differential genes of the RNA-sequencing datasets from SKOV3-con and SKOV3-FXYD5 cell lines were mapped to the Kyoto Encyclopedia of Genes and Genomes pathways. Statistical significance is expressed as a P-value calculated using the right-tailed Fisher's exact test. (B) FXYD5 overexpression or FXYD5 silencing had no effects on TGF-β mRNA expression (upper left and right). FXYD5 overexpression had no effects on TGF-β protein secretion levels in the medium in the SKOV3 cell line (lower left). FXYD5 overexpression had no effects on the mRNA level of *TGFBR1, TGFBR1, SMAD2, SMAD3* and *SMAD4* in the SKOV3 cell line (lower right). (C) Western blotting for the FXYD5, TGF-β receptors and SMAD proteins assessing TGF-β pathway activity in FXYD5-overexpressing and FXYD5-silenced cells. (D) Histograms of the results from (A), (B) and (C). Student's t-test was used to compare quantitative data between two groups, and one-way ANOVA with Dunnett's (D, lower panel) post hoc tests were used to compare the means among multiple groups (n>3). The error bars represent the SD. **P<0.01; ***P<0.001; ns, no significant difference. Con, control; FXYD5, FXYD domain-containing ion transport regulator 5; p-, phosphorylated; TGF-β, transforming growth factor-β; VEGF, vascular endothelial growth factor; PPAR, peroxisome proliferators activated receptor; NK-cell, natural killer cell.

FXYD5 promoted EOC tumor growth and metastasis *in vitro* and *in vivo*.

FXYD5 activates TGF-β/SMADs-induced EMT. To investigate the specific mechanisms that drive EOC metastasis, high-throughput RNA sequencing (Illumina) was performed, using the SKOV3 and SKOV3-IP cell lines with FXYD5 overexpression and FXYD5 deletion, respectively, in combination with a global transcriptome- and pathway-based analysis. Using a minimum fold-change threshold of >2 [Q (adjusted P-value) <0.05], differentially expressed genes were identified (Tables SVIII and SIX). Gene set enrichment analysis indicated that the TGF-β (P=6.12x10-4; Q=0.015) signaling pathway was the most significantly deregulated pathway (according to the enriched gene number and Q value) (Figs. 3A and S2). Therefore, it was speculated that overexpression of FXYD5 may activate the TGF-β signaling pathway.

Subsequently, it was observed that the upregulation of FXYD5 slightly elevated the protein levels of TβR1, whereas it notably increased the phosphorylation of SMAD2 and SMAD3 in the SKOV3 cell line, with no alterations observed in the protein levels of TβR2, SMAD2, SMAD3 and SMAD4 (Fig. 3C). Conversely, FXYD5 deletion notably decreased the TβR1 protein, and SMAD2 and SMAD3 phosphorylation levels in SKOV3-IP cells (Fig. 3C). Additionally, ectopic FXYD5 expression did not induced TGF-β gene transcription or protein secretion, and no alterations were observed in the transcription levels of these TGF-β signaling pathway components (Fig. 3B). These findings suggested that FXYD5 activated TGF-β signaling by elevating the TβR1 protein level.

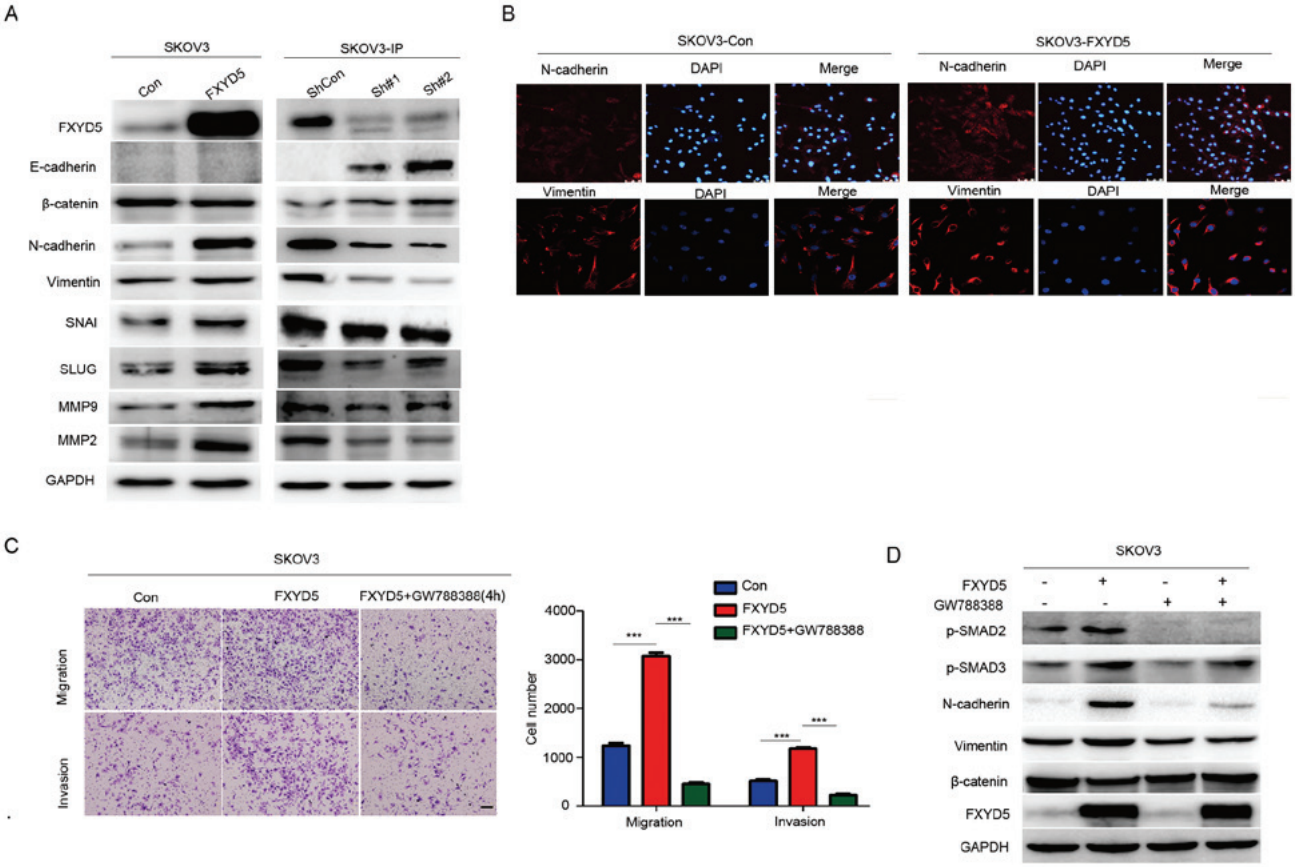

Figure 4. FXYD5 activates EMT by activating TGF-β/SMADs signaling pathway. (A) Western blotting for epithelial (E-cadherin and β-catenin) and mesenchymal (N-cadherin and vimentin) markers to confirm EMT in SKOV3 cells with ectopic FXYD5 expression, and in SKOV3-IP cells with FXYD5 deletion. EMT regulators, including SNAI1, SLUG, MMP9 and MMP2 were examined in SKOV3 and SKOV3-IP cells. (B) Representative images showing overexpressing FXYD5 in SKOV3 cells exhibited decreased levels of epithelial markers, such as E-cadherin, and increased levels of mesenchymal markers, including N-cadherin and vimentin. Scale bar, 10 μm. (C) Transwell assays of cells treated with GW788388 (10 μM) for 48 h and histogram of the results. Magnification, x10. Scale bar, 10 μm. (D) Key markers of the TGF-β signaling pathway and EMT were examined in SKOV3 cells with stable overexpression of FXYD5 treated with GW788388 (10 μM) for 48 h. One-way ANOVA with Least-Significant Difference post hoc tests were used to compare the means among multiple groups (n>3). The error bars represent the SD. ***P<0.001; ns, no significant difference. Con, control; EMT, epithelial-mesenchymal transition; FXYD5, FXYD domain-containing ion transport regulator 5; sh, short hairpin RNA; MMP, matrix metalloproteinase; SNAI, SNAG transcriptional repressor; SLUG, snail family transcriptional repressor 2; TGF-β, transforming growth factor-β.

Notably, enrichment analysis of the data from the RNA-sequencing and TCGA datasets indicated that EMT and EMT-associated processes, including integrin family cell surface interactions, extracellular matrix, intermediate filament and others, were most associated with the FXYD5 alterations (Figs. S3 and 4; Tables SVIII-X). It has been confirmed that TGF-β stimulates EMT, migration, invasion and the metastasis of ovarian cancer cells (Fig. S5A and B) (27). Therefore, it was speculated that FXYD5 may induce EMT and promote EOC metastasis by activating the TGF-β signaling pathway.

Subsequently, through western blotting and immunofluorescence assays, it was demonstrated that the overexpression of FXYD5 resulted in higher N-cadherin and vimentin expression in the SKOV3 cell line (Fig. 4A and B). Among the other EMT biomarkers, β-catenin, another epithelial marker, was downregulated. However, the expression levels of the other mesenchymal markers, including SNAG transcriptional repressor, snail family transcriptional repressor 2, matrix metalloproteinase (MMP)2 and MMP9, were all upregulated, in response to FXYD5 overexpression (Fig. 4A and B). Additionally, in the more mesenchymal-like and metastatic SKOV3-IP cell line, FXYD5 silencing reversed the expression trends of the EMT markers (Fig. 4A) and stimulated mesenchymal-epithelial transition in the cell line. Morphologically, the FXYD5-overexpressing SKOV3 cells became rounded in shape, which is another hallmark of EMT (Fig. 4B).

Additionally, it was revealed that FXYD5 overexpression or treatment of the SKOV3 cells with TGF-β promoted cell migration and invasion, and the ectopic expression of FXYD5 enhanced the effects of TGF-β on cell movements (Fig. S5A and B). Notably, treatment with GW788388, an inhibitor of TGF-β/SMADs signaling (28), reversed the effects of ectopic FXYD5 on cell migration, invasion and EMT (Fig. 4C and D). Overall, these results suggested that FXYD5 potentiated TGF-β/SMADs signaling and TGF-β-induced EMT in ovarian cancer cells.

FXYD5 maintains the continuous activation of TGF-β/SMAD signaling by suppressing TβR1 degradation. Notably, TβR1 protein, but not mRNA alterations, were observed in response to FXYD5 alterations (Fig. 3B and C). Therefore, it was proposed that the loss of FXYD5 would predominantly degrade the TβR1 protein in a post-transcriptional manner. To confirm this hypothesis, the SKOV3 cells overexpressing

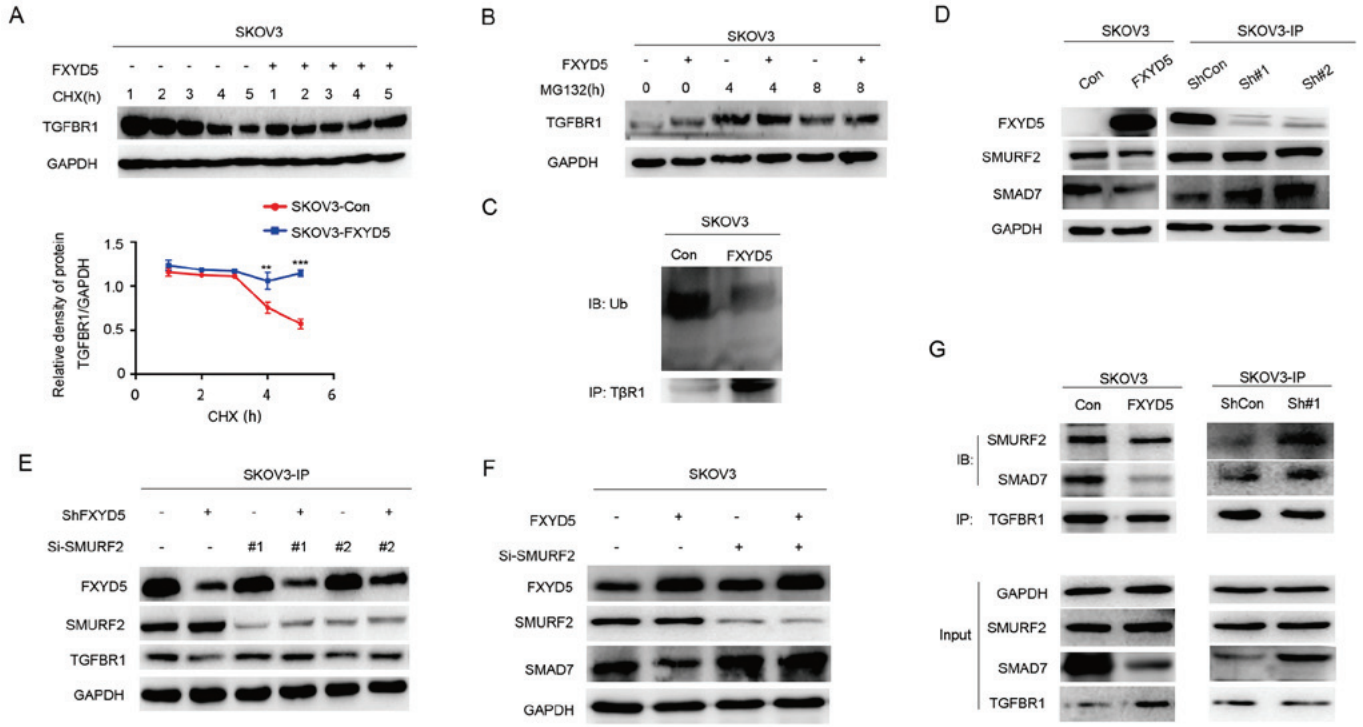

Figure 5. FXYD5 activates the TGF-β/SMADs signaling pathway via suppressing TβR1 degradation. TGFBR1 expression by IB analysis in SKOV3-Con and SKOV3-FXYD5 cells treated with (A) CHX (100 μg/ml) and (B) MG132 (10 μM) for the indicated lengths of time. (C) SKOV3-Con and SKOV3-FXYD5 cells were treated with 10 μM MG132 for 4 h. Following cell harvest, proteins were immunoprecipitated with an anti-TβR1 antibody and detected using a polyubiquitin antibody. (D) WB analysis of SMRF2 and SMAD7 in FXYD5-overexpressing SKOV3 and FXYD5-silenced SKOV3-IP cells. WB analysis of TβR1 and SMAD7 in (E) FXYD5-silenced SKOV3-IP and (F) FXYD5-overexpressing SKOV3 cells after being treated with si-SMURF2 and Si-Control plasmid vectors for 48 h. (G) Lysates of FXYD5-overexpressing SKOV3 and FXYD5-silenced SKOV3-IP cells were subjected to anti-TβR1 IP followed by IB with anti-SMAD7 and anti-SMURF2. Statistical analysis was performed using Student's t-test (n≥3). The error bars represent the SD. **P<0.01; ***P<0.001; TGFBR1, TGF-β receptor 1; IB, immunoblotting; WB, western blotting; IP, immunoprecipitation; Con, control; FXYD5, FXYD domain-containing ion transport regulator 5; Ub, ubiquitin; sh, short hairpin RNA; SMURF2, SMAD specific E3 ubiquitin protein ligase 2; si, small interfering RNA.

FYXD5 were incubated with CHX, an inhibitor of protein biosynthesis. Compared with the control group (SKOV3-Con), and according to the curve shown in Fig. 5A, TβR1 protein was markedly degraded at a slower rate, and even increased within 6 h of the CHX treatment in the FXYD5-overexpressing group (SKOV3-FXYD5; Fig. 5A). Furthermore, treatment of these cells with MG132, a proteasome inhibitor, increased the stable TβR1 protein level (Fig. 5B). Additionally, in the SKOV3-FXYD5 cell lines, poly-ubiquitination of TβRI was reduced (Fig. 5C), indicating that TβR1 protein degradation is directed by the ubiquitin-proteasome system.

As shown in Fig. 5D, the ectopic expression of FXYD5 markedly decreased SMAD7 expression in the SKOV3 cells. Conversely, FXYD5 silencing led to a marked increase in SMAD7 expression in the SKOV3-IP cells (Fig. 5D). However, FXYD5 silencing had no effect on SMURF2 expression in the SKOV3-IP cell line (Fig. 5D). To further examine whether SMURF2 was involved in this process, an effective small interfering RNA (si-)SMURF2 construct was generated to knockdown SMURF2, and it was revealed that si-SMURF2 significantly reversed the degrading effects of FXYD5 deletion on TβR1 and the derogation of SMAD7 induced by FXYD5 overexpression (Fig. 5E and F), suggesting that SMURF2 was required for FXYD5-mediated TβR1 and SMAD7 alterations. Furthermore, IP assays demonstrated that sh-FXYD5 promoted the binding of SMURF2 and SMAD7 to TβR1, whereas FXYD5 inhibited these interactions (Fig. 5G). These results demonstrated that FXYD5 upregulation dispersed the SMAD7-SMURF2-TβR1 complex, promoted the deubiquitination and stabilization of TβR1, and activated tTGF-β/SMADs signaling. The SMAD7 protein may also be degraded by the ubiquitin-proteasome system in response to FXYD5 upregulation, which requires further investigation.

TGF-β-activated SMAD3/4 complex upregulates FXYD5 expression. Notably, positive correlations were identified between the FXYD5 and TGFB1 and the FXYD5 and TGFB1I1 mRNA levels in the patients with ovarian cancer from the two datasets from TCGA (Figs. 6A and S3D; Table SX). Additionally, TGFB1 and TGFB1I1 were also positively co-expressed in the two TCGA datasets (Fig. S5D). As aforementioned, FXYD5 did not induce either TGF-β gene transcription or protein secretion (Fig. 3B). Therefore, it was proposed that activated TGF-β signaling could induce FXYD5 expression. SKOV3 cells were treated with various concentrations of TGF-β (0-10 ng/ml) for 24 h (Fig. S5E). As shown in Figs. S3E and 6B, the TGF-β treatment upregulated the FXYD5 mRNA and protein levels in a dose- and time-dependent manner. Inversely, treatment with GW788388, an inhibitor of TGF-β/Smad3 signaling, abolished the effects of TGF-β on FXYD5 expression (Fig. S5F-H).

To examine whether the SMAD signaling pathway is required for TGF-β-induced FXYD5 upregulation in human ovarian cancer cells, SMAD signaling transduction was

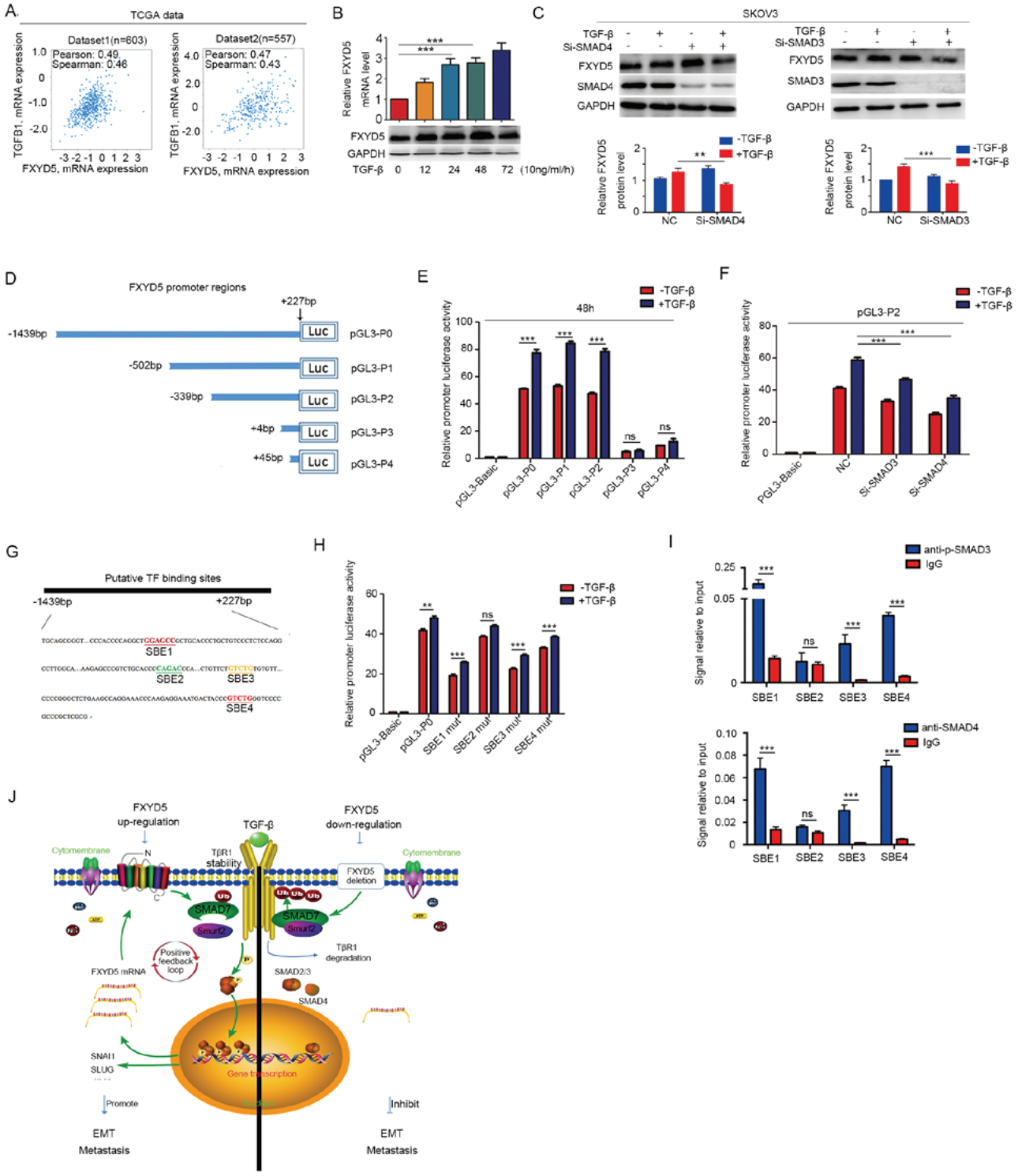

Figure 6. TGF-β-activated SMAD3/4 complex is recruited to FXYD5 promoter and binds to SBEs to enhance transcription. *TGFB1* was co-expressed with *FXYD5* in two TCGA datasets. Correlation values and P-values were determined using Spearman and Pearson's correlation. (B) *FXYD5* mRNA and protein levels in SKOV3 cells in the presence of TGF-β (10 ng/ml) for the indicated times. (C) WB analysis of FXYD5 expression in SKOV3 cells treated with si-SMAD4 and si-SMAD3, in the absence or presence of TGF-β for 48 h. (D) A series of truncated FXYD5-promoter luciferase constructs were generated according to the predicted SMAD2-SMAD3-SMAD4 complex binding sites for the FXYD5 promoter in the Jaspar (http://jaspar.genereg.net). (E) 293T cells were transiently transfected with the constructs indicated in (D), and then treated with or without TGF-β (10 ng/ml) for 48 h. Subsequently, their luciferase activities were tested. (F) Luciferase activity of PGL-P2 promoter in 293T cells that were transfected with NC, si-SMAD3 and si-SMAD4 in the absence or presence of TGF-β for 48 h. (G) Computational algorithms by use of TFSEARCH (http://www.cbrc.jp/research/db/TFSEARCH) predicted that the PGL-P0 promoter region harbored four putative protein-binding sites (SBE1-4), which were shown in different colors. (H) 293T cells were transfected with the constructs including the wild type or mutant type of the putative binding sites, which were indicated in (G), and then the luciferase activities were assessed in the absence or presence of TGF-β (10 ng/ml) for 48 h. (I) Chromatin immunoprecipitation assays using antibodies against p-SMAD3 and SMAD4 were utilized to determine the enrichment degree of the FXYD5 promoter containing SBEs in 293T cells upon TGF-β stimulation. (J) A positive feedback loop for the regulation of TGF-β-induced EMT by FXYD5. Student's t-test was used to compare quantitative data between two groups, and one-way ANOVA with Least-Significant Difference post hoc tests were used to compare the means among multiple groups (n>3). The error bars represent the SD. **P<0.01; ***P<0.001; ns, no significant difference. SBE, SMAD-binding elements; TCGA, The Cancer Genome Atlas; TGF-β, transforming growth factor-β; FXYD5, FXYD domain-containing ion transport regulator 5; WB, western blotting; si, small interfering RNA; NC, negative control; p-, phosphorylated; IgG, immunoglobulin G; EMT, epithelial-mesenchymal transition.

blocked by the siRNA-mediated knockdown of common SMAD4. As shown in Fig. 6C, the SMAD4 siRNA significantly downregulated endogenous SMAD4 expression, and the TGF-β-induced elevation of the FXYD5 protein levels was abolished by SMAD4 silencing. To further determine which SMAD was required for TGF-β-induced FXYD5 expression, a specific siRNA was used to knockdown SMAD2 or SMAD3 in SKOV3 cells. As shown in Figs. 6C and S3I, the silencing of SMAD3 alone, but not that of SMAD2, attenuated TGF-β-induced upregulation of the FXYD5 protein levels. Hence, it was hypothesized that the SMAD3/SMAD4 complex mediates FXYD5 transcription by binding to the promoter region of the FXYD5 gene.

Identification of the TGF-β response regions that contain putative functional SBEs in the FXYD5 promoter. To identify the role of activated TGF-β signaling in regulating FXYD5 promoter transcription, a DNA fragment between -1,439 and +227 relative to the FXYD5 transcription start site (TSS) was cloned into a pGL3-Basic plasmid to yield a pGL3-TGF-β recombinant vector that could deliver the FXYD5 promoter (Fig. 6D and E). Sequence constructs P0, P1 and P2 increased the luciferase activity level in the 293T cells; however, sequence constructs P3 and P4 exhibited luciferase activity levels that were equivalent to those of the control (Fig. 6E). This result indicated that activated TGF-β signaling increased the transcriptional activity of the FXYD5 promoter by binding to the region that was located between -1439 and +4 relative to the TSS (Fig. 6D and E). Furthermore, it was observed that the luciferase activity of the P2 promoter was significantly decreased in the 293T cells in which SMAD3 and SMAD4 were silenced and which were treated with TGF-β (Fig. 6F). These results suggested that the TGF-β-activated SMAD3/4 complex may have the capacity to bind to the FXYD5 promoter and initiate FXYD5 transcription.

Furthermore, using TFSEARCH, four putative transcriptional factor binding sites, including SBE1, SBE2, SBE3 and SBE4, that were located in the -1439/+4 FXYD5 promoter region, were identified (Fig. 6G). Subsequently, various luciferase reporter constructs containing the wild-type and mutant forms of the four TF-binding sites were transfected into the 293T cells. Upon TGF-β stimulation, three constructs exhibited significantly decreased luciferase activities compared with those of the wild-type construct; the mutant construct of the SBE2-binding site was the exception (Fig. 6H). As the TGF-β-activated SMAD3/4 complex can be recruited to SBEs (29,30), the findings suggested the possibility that the TGF-β-activated SMAD3/4 complex may positively regulate the transcription of FXYD5 by binding to SBE1, SBE3 and SBE4.

Finally, the ChIP assays revealed that upon TGF-β stimulation, the SMAD-binding elements in the FXYD5 promoter, including SBE1, SBE3 and SBE4, were more enriched in the immunoprecipitates that were obtained using the corresponding antibodies (Fig. 6I).

Collectively, these results indicated that the TGF-β-activated SMAD3/SMAD4 complex was directly recruited to the FXYD5 promoter region and that the complex interacted with specific SBEs, thus promoting FXYD5 transcription.

Discussion

Our previous study screened and identified a set of miRNAs, including let-7a, let-7e, let-7f, miR-22 and miR-886-5p, from the SKOV3 ovarian cancer cell line and from SKOV3-IP, the metastatic subline of SKOV3, as the most significant potential suppressor genes associated with ovarian cancer invasion and metastasis (26,31,32). The present study, utilizing bioinformatics analysis, identified FXYD5 as the common target gene of these miRNAs. Therefore, it was speculated that FXYD5 may serve a promotor role during EOC progression.

The present study demonstrated that FXYD5 was upregulated in metastatic ovarian cancer, and that it was associated with a worse patient survival. Extensive functional analyses confirmed its metastasis promoter role *in vitro*. Mechanistically, by affecting the SMURF2-SMAD7 complex in regulating the TβR1 protein level, FXYD5 positively regulated TGF-β/SMAD signaling activities, which in turn induced FXYD5 expression via the activated SMAD3/4 complex, creating a positive feedback loop and driving the cells to undergo the EMT mediated metastasis in ovarian cancer (Fig. 6J).

The present study revealed that FXYD5 was substantially upregulated in the more aggressive subline, SKOV3-IP, which was developed from the parental SKOV3 cells by *in vivo* selection in mice (26). Accordingly, the SKOV3-IP cells exhibited an increased invasiveness compared with the parental SKOV3 cells. Due to the similar genetic background of these cells, they provide a unique model for identifying candidate metastasis-associated biomarkers and potential therapeutic targets for EOC.

Previous data from a large-scale high-throughput analysis of numerous high-grade serous ovarian cancer samples suggested that the high invasive propensity of ovarian cancer cells is coupled with a TGF-β gene signature (3,29). The results of the present study first linked FXYD5 to TGF-β signaling. Positive feedback is renowned to magnify a signal and facilitates a self-maintaining mode, which is autonomous to the initial inducements. It was hypothesized that, once activated by TGF-β, the FXYD5-mediated feedback loop would enable EOC cells to become self-governing, which would reinforce the propensity of the EOC cells to invade and metastasize to new microenvironments, and would explain the co-expression and significant upregulation of FXYD5 and TGF-β in late-stage EOC (4,5).

To date, to the best of our knowledge, no additional partners for interaction have been described for FXYD5, apart from for the Na^+/K^+-ATPase subunits (14,33). Previous studies have demonstrated that the SMAD7-SMURF2 complex is recruited to the TGF-β receptor complex, where it results in the ubiquitination and degradation of the receptors as well as SMAD7 via the proteasome-mediated signaling pathway (9,34). Kavsak *et al* (9) have defined SMAD7 as an adaptor in an E3 ubiquitin ligase complex that targets the TGF-ß receptor for degradation. The present study demonstrated that FXYD5 not only downregulated the SMAD7 protein expression levels, but also dispersed the SMAD7-SMURF2 complex, which can be recruited to the TGF-β receptor, where it de-ubiquitinates and stabilizes TβR1 (9,10,34,35). Therefore, the post-transcriptional regulation of SMAD7 or regulation of the stability of the SMAD7-SMURF2 complex by FXYD5 may serve an

important role in the progression of ovarian cancer and in TGF-β signaling. However, the detailed mechanisms though which FXYD5 regulates SMAD7 and the SMAD7-SMURF2 complex, whether through the Na^+/K^+-ATPase or not, requires further investigation. Additionally, the problem that the TGFβR1 expression at 1-3 h in the FXYD5(-) group was significantly higher than that in the FXYD5(+) group was noted. Since GAPDH expression at 1-3 h in the FXYD5(-) group was also significantly higher than that in the FXYD5(+) group; it was likely that the aforementioned results were caused by the difference in the amount of the total protein samples. Therefore, TGFBR1 protein expression was normalized based on GAPDH protein expression. Furthermore, according to the ratio of TGFBR1 to GAPDH over time, the curve was made to compare the degradation rates of TGFBR1 protein between the FXYD5(+) and FXYD5(-) groups. In the curve shown in Fig. 5A, there was no significant difference at the initial 1-3 h; however, the FXYD5(+) group exhibited a slower degradation rate at 4-6 h.

The TGF-β signaling pathway is currently viewed as a therapeutic target in advanced tumors (36). To disrupt this intriguing feedback loop, FXYD5 represents an ideal target. As a transmembrane protein that is located in the cytomembrane, the unusually long extracellular domain of FXYD5 (15) may enable the design of a homing target for immunotoxins or cancer-directed imaging agents. Additionally, the survival analysis indicated that for patients undergoing chemotherapy, high FXYD5 expression as associated with poor survival. Therefore, in addition to these chemotherapeutic strategies, FXYD5 may be an alternative therapeutic target that can extend the survival time of patients.

Due to the tumor heterogeneity, there are marked differences in molecular biological behaviors between different tumors. Whether this feedback loop exists in other tumors remains to be explored. In the future it should be explored whether this feedback loop could be applied to other types of cancer, including cervical cancer, breast cancer and lung cancer.

In summary, the results identified FXYD5 as a novel metastasis driver, thus elucidating the mechanisms that underlie the TGF-β/SMADs signaling pathway in ovarian cancer, and providing a promising therapeutic target for human ovarian cancer.

Acknowledgements

Not applicable.

Funding

The present study was supported by grants from Shanghai Sailing Program (grant nos. 16YF1401100 and 19YF1404300), Natural Science Foundation of Shanghai (grant no. 17ZR1403500) and Natural Science Foundation of China (grant no. 81802596).

Availability of data and materials

The datasets used and/or analyzed during the current study are available from the corresponding author on reasonable request.

Authors' contributions

YB collected the clinical samples and patient information, and conducted the majority of *in vitro* and *in vivo* experiments. LDL conducted the bioinformatics analysis, immunohistochemistry staining and survival analysis. JL, RFC and HLY helped establishing the stable cell lines and participated in *in vitro* experiments on functions. HFS and JYW participated in western blot analysis and made constructs. YB, LDL and XL conceived the project, designed most of the experiments and wrote the manuscript. XL supervised the project. All authors have read and approved the final manuscript.

Ethics approval and consent to participate

Approval was obtained from the Human Research Ethics Committee of the Obstetrics and Gynecology Hospital of Fudan University for the use of all samples by using a protocol that conforms to the provisions of the Declaration of Helsinki (as revised in Seoul, 2008; reference no. [2015] 27). Written informed consent was obtained from all patients. Animal experiments were approved by the Institutional Animal Care and Use Committee of Fudan University.

Patient consent for publication

Not applicable.

Competing interests

The authors declare that they have no competing interests.

References

1. Lengyel E: Ovarian cancer development and metastasis. Am J Pathol 177: 1053-1064, 2010.
2. Ye X and Weinberg RA: Epithelial-mesenchymal plasticity: A central regulator of cancer progression. Trends Cell Biol 25: 675-686, 2015.
3. Yang D, Sun Y, Hu L, Zheng H, Ji P, Pecot CV, Zhao Y, Reynolds S, Cheng H, Rupaimoole R, *et al*: Integrated analyses identify a master microRNA regulatory network for the mesenchymal subtype in serous ovarian cancer. Cancer Cell 23: 186-199, 2013.
4. Parikh A, Lee C, Joseph P, Marchini S, Baccarini A, Kolev V, Romualdi C, Fruscio R, Shah H, Wang F, *et al*: MicroRNA-181a has a critical role in ovarian cancer progression through the regulation of the epithelial-mesenchymal transition. Nat Commun 5: 2977, 2014.
5. Matsumura N, Huang Z, Mori S, Baba T, Fujii S, Konishi I, Iversen ES, Berchuck A and Murphy SK: Epigenetic suppression of the TGF-beta pathway revealed by transcriptome profiling in ovarian cancer. Genome Res 21: 74-82, 2011.
6. Wang Y, Shi J, Chai K, Ying X and Zhou BP: The role of Snail in EMT and tumorigenesis. Curr Cancer Drug Targets 13: 963-972, 2013.
7. Ikushima H and Miyazono K: TGFbeta signalling: A complex web in cancer progression. Nat Rev Cancer 10: 415-424, 2010.
8. Peinado H, Olmeda D and Cano A: Snail, Zeb and bHLH factors in tumour progression: An alliance against the epithelial phenotype? Nat Rev Cancer 7: 415-428, 2007.
9. Kavsak P, Rasmussen RK, Causing CG, Bonni S, Zhu H, Thomsen GH and Wrana JL: Smad7 binds to Smurf2 to form an E3 ubiquitin ligase that targets the TGF beta receptor for degradation. Mol Cell 6: 1365-1375, 2000.
10. Eichhorn PJ, Rodón L, Gonzàlez-Juncà A, Dirac A, Gili M, Martínez-Sáez E, Aura C, Barba I, Peg V, Prat A, *et al*: USP15 stabilizes TGF-β receptor I and promotes oncogenesis through the activation of TGF-β signaling in glioblastoma. Nat Med 18: 429-435, 2012.

11. Lee YK, Lee SY, Park JR, Kim RJ, Kim SR, Roh KJ and Nam JS: Dysadherin expression promotes the motility and survival of human breast cancer cells by AKT activation. Cancer Sci 103: 1280-1289, 2012.
12. Lubarski I, Asher C and Garty H: FXYD5 (dysadherin) regulates the paracellular permeability in cultured kidney collecting duct cells. Am J Physiol Renal Physiol 301: F1270-F1280, 2011.
13. Lubarski I, Asher C and Garty H: Modulation of cell polarization by the Na^+-K^+-ATPase-associated protein FXYD5 (dysadherin). Am J Physiol Cell Physiol 306: C1080-C1088, 2014.
14. Lubarski-Gotliv I, Dey K, Kuznetsov Y, Kalchenco V, Asher C and Garty H: FXYD5 (Dysadherin) may mediate metastatic progression through regulation of the beta- Na^+-K^+-ATPase subunit in 4T1 mouse breast cancer model. Am J Physiol Cell Physiol 313: C108-C117, 2017.
15. Lubarski I, Pihakaski-Maunsbach K, Karlish SJ, Maunsbach AB and Garty H: Interaction with the Na,K-ATPase and tissue distribution of FXYD5 (related to ion channel). J Biol Chem 280: 37717-37724, 2005.
16. Lubarski I, Karlish SJ and Garty H: Structural and functional interactions between FXYD5 and the Na^+-K^+-ATPase. Am J Physiol Renal Physiol 293: F1818-F1826, 2007.
17. Nam JS, Kang MJ, Suchar AM, Shimamura T, Kohn EA, Michalowska AM, Jordan VC, Hirohashi S and Wakefield LM: Chemokine (C-C motif) ligand 2 mediates the prometastatic effect of dysadherin in human breast cancer cells. Cancer Res 66: 7176-7184, 2006.
18. Raman P, Purwin T, Pestell R and Tozeren A: FXYD5 is a marker for poor prognosis and a potential driver for metastasis in ovarian carcinomas. Cancer Inform 14: 113-119, 2015.
19. Lubarski Gotliv I: FXYD5: Na(+)/K(+)-ATPase regulator in health and disease. Front Cell Dev Biol 4: 26, 2016.
20. Cerami E, Gao J, Dogrusoz U, Gross BE, Sumer SO, Aksoy BA, Jacobsen A, Byrne CJ, Heuer ML, Larsson E, *et al*: The cBio cancer genomics portal: An open platform for exploring multidimensional cancer genomics data. Cancer Discov 2: 401-404, 2012.
21. Gyorffy B, Lánczky A and Szállási Z: Implementing an online tool for genome-wide validation of survival-associated biomarkers in ovarian-cancer using microarray data from 1287 patients. Endocr Relat Cancer 19: 197-208, 2012.
22. McCarty KS Jr, Miller LS, Cox EB, Konrath J and McCarty KS Sr: Estrogen receptor analyses. Correlation of biochemical and immunohistochemical methods using monoclonal antireceptor antibodies. Arch Pathol Lab Med 109: 716-721, 1985.
23. Livak KJ and Schmittgen TD: Analysis of relative gene expression data using real-time quantitative PCR and the 2(-Delta Delta C(T)) Method. Methods 25: 402-408, 2001.
24. Jiang HL, Sun HF, Gao SP, Li LD, Huang S, Hu X, Liu S, Wu J, Shao ZM and Jin W: SSBP1 suppresses TGFβ-driven epithelial-to-mesenchymal transition and metastasis in triple-negative breast cancer by regulating mitochondrial retrograde signaling. Cancer Res 76: 952-964, 2016.
25. Pathan M, Keerthikumar S, Ang CS, Gangoda L, Quek CY, Williamson NA, Mouradov D, Sieber OM, Simpson RJ, Salim A, *et al*: FunRich: An open access standalone functional enrichment and interaction network analysis tool. Proteomics 15: 2597-2601, 2015.
26. Yu D, Wolf JK, Scanlon M, Price JE and Hung MC: Enhanced c-erbB-2/neu expression in human ovarian cancer cells correlates with more severe malignancy that can be suppressed by E1A. Cancer Res 53: 891-898, 1993.
27. Vergara D, Merlot B, Lucot JP, Collinet P, Vinatier D, Fournier I and Salzet M: Epithelial-mesenchymal transition in ovarian cancer. Cancer Lett 291: 59-66, 2010.
28. Petersen M, Thorikay M, Deckers M, van Dinther M, Grygielko ET, Gellibert F, de Gouville AC, Huet S, ten Dijke P and Laping NJ: Oral administration of GW788388, an inhibitor of TGF-beta type I and II receptor kinases, decreases renal fibrosis. Kidney Int 73: 705-715, 2008.
29. Yang H, Wang L, Zhao J, Chen Y, Lei Z, Liu X, Xia W, Guo L and Zhang HT: TGF-β-activated SMAD3/4 complex transcriptionally upregulates N-cadherin expression in non-small cell lung cancer. Lung Cancer 87: 249-257, 2015.
30. Shi Y, Wang YF, Jayaraman L, Yang H, Massagué J and Pavletich NP: Crystal structure of a Smad MH1 domain bound to DNA: Insights on DNA binding in TGF-beta signaling. Cell 94: 585-594, 1998.
31. Liang SH, Li J, Al-beit M, Zhang J, Ma D and Lu X: Screening and identification of potential miRNA involved in ovarian cancer invasion and metastasis. Zhonghua Zhong Liu Za Zhi 32: 650-654, 2010 (In Chinese).
32. Bai F, Feng J, Cheng Y, Shi J, Yang R and Cui H: Analysis of gene expression patterns of ovarian cancer cell lines with different metastatic potentials. Int J Gynecol Cancer 16: 202-209, 2006.
33. Antonov AV, Krestyaninova M, Knight RA, Rodchenkov I, Melino G and Barlev NA: PPISURV: A novel bioinformatics tool for uncovering the hidden role of specific genes in cancer survival outcome. Oncogene 33: 1621-1628, 2014.
34. Ogunjimi AA, Briant DJ, Pece-Barbara N, Le Roy C, Di Guglielmo GM, Kavsak P, Rasmussen RK, Seet BT, Sicheri F and Wrana JL: Regulation of Smurf2 ubiquitin ligase activity by anchoring the E2 to the HECT domain. Mol Cell 19: 297-308, 2005.
35. Jiang HL, Sun HF, Gao SP, Li LD, Hu X, Wu J and Jin W: Loss of RAB1B promotes triple-negative breast cancer metastasis by activating TGF-β/SMAD signaling. Oncotarget 6: 16352-16365, 2015.
36. Akhurst RJ and Hata A: Targeting the TGFβ signalling pathway in disease. Nat Rev Drug Discov 11: 790-811, 2012.